# Trapping effect and trajectory control of surface plasmon polaritons in a metal-dielectric-metal waveguide

Yong Zhou,[1] Qi Liu,[2,3] Chuan-kui Wang,[1] and Chaohua Tan[1,*]

[1]*School of Physics and Electronics, Shandong Normal University, Jinan 250014, China*

[2]*State Key Laboratory for Mesoscopic Physics, Department of Physics, Peking University, Beijing 100871, China*

[3]*Beijing Academy of Quantum Information Sciences, Beijing 100193, China*

(Received 5 February 2020; accepted 30 November 2020; published 11 December 2020)

A nonlinear optical-magnetic manipulation scheme is proposed to realize the low-loss surface plasmon polaritons (SPPs) trapping in metal-dielectric-metal (MDM) waveguide, based on double electromagnetically induced transparency (EIT) and cross-phase modulation (CPM), theoretically. Using incoherent pumping, the Ohmic loss of SPPs is compensated. The huge nonlinearity in the system balances the diffraction of the SPPs, and a SPPs soliton is obtained. With the SPPs solitons, we realize the trapping of another weaker SPPs via CPM. We find that the trapped SPPs have a similar profile as the stronger SPPs, thus, the profile of trapped SPPs can be controlled even can be focused when being defused. We also show that the SPPs will deflect in an external gradient magnetic field, and the trajectory of the SPPs can be manipulated dynamically via adjusting the magnetic field gradient. The results obtained here may have great potential in future on-chip circuitry.

DOI: 10.1103/PhysRevA.102.063516

## I. INTRODUCTION

On-chip circuitry in optics version is attractive for developing next generation high speed communication and computing technology [1]. Surface plasmon polaritons (SPPs) can highly confine the electromagnetic field into the subwavelength scale near the metal-dielectric interface, thus, it provide a effective method to integrate the light into chip [2]. Recently, many plasmonic devices such as ultrafast switch [3], splitters [4], logic gates [5], etc. have been designed to construct such an optical circuitry, and the researches in this field even have been extended the research to quantum level [6].

One of the key points to realize the optical circuitry is to manipulate SPPs effectively. Such manipulation is mainly about controlling the propagation properties of the SPPs. On the one hand, loss and diffraction nature will hugely reduce the intensity of SPPs, which can be used to modulate the SPPs signal intensity [7]. On the other hand, the propagation trajectory of SPPs signal also deserves to manipulate, which is important for constructing some functional devices like SPPs router [8,9].

In recent years, many methods have been developed to meet the two aspects. The plasmonic and hybrid waveguides are ideal to guide the SPPs, and the route to guide SPPs can be designed, and with the help of so called active plasmonic technology [2,7], the loss of SPPs become controllable via adjusting additional field applied to the system, such as temperature [10], voltage [11,12], magnetic field [13], and so on. Special waveguide array can create an inhomogeneous transverse reflect index environment and induces a zigzag trajectory of SPPs [14,15]. Further more, the SPPs can be manipulated by designing the exciting structure and controlling the properties of incident light (such as polarization, incident angle) in waveguide system [16–19]. The discovery of nondiffraction SPPs beams [20] enrich the method to manipulate SPPs. For example, the Airy SPPs beam, not only being nondiffracting but also self-healing [21], thus, the loss of SPPs reduced, and it has a controllable bending trajectory related to the incident condition [22–24]. Coupling SPPs to quantum system is also an alternative way to manipulate SPPs. The application of electromagnetically induced transparency (EIT) [25] technic and negative-index metamaterial (NIMM) interface largely enhance the nonlinearity response of SPPs, thus, it generates a great platform for nonlinear manipulation of the tightly confined electromagnetic wave like SPPs [26], SPs (surface polaritons, a kind of tightly confined EM mode similar to SPPs) [27–30]. With the platform, the low-loss nonlinear SPPs or SPs such as solitons [31–33], rogue wave, breather, and frequency comb [34,35] can be generated, the diffraction effect can be balanced with the huge nonlinearity, and the spatial control can be realized.

Most of the methods we mentioned above are inspired from the methods to manipulate light in free space or fiber, and have make great progress in controlling SPPs. Other methods such as soliton radiation trapping [36–38] (i.e., trapping light by light), Stern-Gelach-like effect of light [39–41] (i.e., deflect light via gradient magnetic field), are also useful to manipulate the trajectory of week light signal. However, using such methods to manipulate SPPs seem have not arisen enough attention of researchers.

In this paper, we propose to adopt a metal-dielectric-metal (MDM) waveguide based platform to manipulate SPPs, and based on it, we theoretically investigate the trapping effect and trajectory control of SPPs via EIT effect and external magnetic field. We apply the incoherence pump technic, and

*tanch@sdnu.edu.cn

 

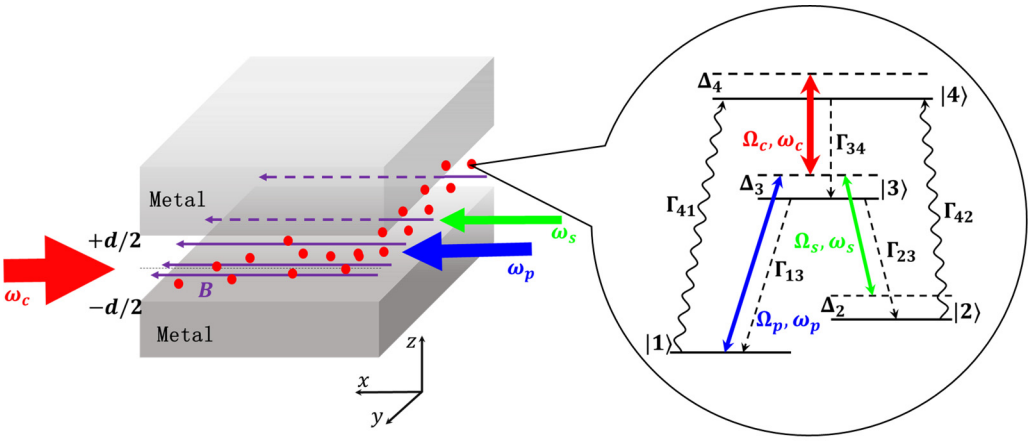


(a) (b)

FIG. 1. (a) MDM waveguide system to manipulate SPPs. A strong control field (red arrow, along the $-x$ direction), weak probe field (blue arrow, along the $x$ direction), and weaker signal field (green arrow, along the $x$ direction) are incident, and SPPs are excited. The dielectric layer is hot atomic vapors (red points) interacting with the three SPPs fields. A inhomogeneous magnetic field with gradient in the $y-$ direction is applied to the system to manipulate the SPPs. (b) Energy level configuration of atoms. $\Delta_j (j = 2, 3, 4)$ is detuning, $\Gamma_{ij}$ is spontaneous emission decay rate(for $i < j$) or incoherent pumping rate(for $i > j$), $\Omega_j$ and $\omega_j$ $(j = c, p, s)$ are, half-Rabi frequency and center frequency, respectively.

realize the low-loss propagation for both symmetric and antisymmetric SPPs modes. Then, we obtain a shape-preserving probe SPPs due to the strong nonlinearity in the system. Furthermore, we show that a weaker signal SPPs can be trapped by the probe SPPs soliton via cross-phase modulation, and the trapped SPPs has a similar profile as the probe one, which can be used to focus the defused signal SPPs or reshape it. Our numerical results also suggest that the trapping effect is still valid when a transverse gradient magnetic field is applied to the system, and the SPPs will deflect in the magnetic field, thus, the trajectory of SPPs can be controlled. A real time trajectory control is realized using a time-dependent gradient magnetic field.

The article is arranged as follows. In the next section, we describe the theoretical model. In Secs. III and IV, the linear and nonlinear properties of SPPs in our system are analyzed, respectively. In Sec. V, we study the manipulation of the SPPs based on CPM and the external magnetic field. In the last section, we summarize the main results obtained in this work.

## II. THEORETICAL MODEL

We consider a MDM waveguide system, as shown in Fig. 1(a). For convenience of theoretical analyzing, we assume the geometry configuration of the waveguide system is extended to infinity both in the $y$ and $z$ directions. The dielectric with permittivity $\varepsilon_1$ and permeability $\mu_1$ has a thickness $d$ in the $z$ direction. And the covered layers in both side of the dielectric are the same metal with permittivity $\varepsilon_2$ and permeability $\mu_2$. The dielectric layer adopted here is hot atomic vapors, and atoms in which have an inverted-Y-type four-level configuration. As illustrated in Fig. 1(b), the energy levels of the atoms are two ground states $|1\rangle$ and $|2\rangle$ and one intermediate state $|3\rangle$ and one upper state $|4\rangle$. Three laser fields (control, probe and signal) are guided in the MDM waveguide with TM SPPs mode, and interacting with the atoms. The probe and signal fields propagate along the $x$ direction, and the control field propagates along the $-x$ direction, such a scheme can suppress the first-order Doppler effect [42]. $\omega_c$, $\omega_p$ and $\omega_s$ are center frequency of the control, probe and signal fields, respectively. The strong control field drives the transition $|3\rangle \leftrightarrow |4\rangle$ with half-Rabi frequency $\Omega_c$, while the weak probe field drives the transition $|1\rangle \leftrightarrow |2\rangle$ with half-Rabi frequency $\Omega_p$, and the weaker signal field drives the transition $|2\rangle \leftrightarrow |3\rangle$ with half-Rabi frequency $\Omega_s$. $\Gamma_{jl} (j < l, l = 3, 4)$ is the spontaneous emission decay rate from state $|l\rangle$ to state $|j\rangle$, $\Gamma_{4l} (l = 1, 2)$ is the incoherent pumping, and $\Delta_k (k = 2, 3, 4)$ is the detuning.

As shown in Ref. [43], the MDM waveguide system only support transverse-magnetic (TM) SPPs modes, and two TM modes (symmetric and antisymmetric) can be found from Maxwell equations, which satisfied the boundary conditions at metal-dielectric interface (as well as boundary conditions at $z = \pm\infty$), and the dispersion relation of TM mode in MDM waveguide is given by

$$\tanh\left(\frac{k_{z1}d}{2} + \psi\right) = -\frac{\varepsilon_1}{\varepsilon_2}\frac{k_{z2}}{k_{z1}}, \tag{1}$$

where $k_{zj}^2 = k^2 - \varepsilon_j \mu_j k_0^2$ ($j = 1$ for the dielectric and $j = 2$ for the metal), $\psi = m\pi i/2$ ($i$ is imaginary unit, $m = 0$ for symmetric mode and $m = 1$ for antisymmetric mode), $k_0$ is the wave number in vacuum and $k$ is the propagation constant of SPPs. When we discuss symmetry in this paper, we are referring the symmetry of magnetic field profile with respect to the center plain of the dielectric layer in MDM configuration. Equation (1) gives a complex propagation constant for both symmetric and antisymmetric mode due to the Ohmic loss of the metal, thus the weak probe and signal fields could not propagate for a relatively long distance. To compensate the loss, we introduce incoherent pumping to our system, which pump the ground states $|1\rangle$ and $|2\rangle$ to upper state $|4\rangle$ with pumping rate $\Gamma_{41}$ and $\Gamma_{42}$, respectively.

The electric fields interacting with the atoms read

$$\mathbf{E}(\mathbf{r},t)=\sum_{l=c,p,s}\mathcal{E}_l\mathbf{u}_l(z)e^{i(k(\omega_l)x-\omega_l t)}+\text{c.c.}, \tag{2}$$

where $\mathbf{u}_l(z)=(k(\omega_l)\cosh(k_{z1}z+\psi)\mathbf{e}_z+ik_{z1}(\omega_l)\sinh(k_{z1}z+\psi)\mathbf{e}_x)/k(\omega_l)$ is the mode function in the $z$ direction, and $\mathcal{E}_l$ is the amplitude envelope function of the electric field. To investigate the trapping effect and the trajectory control of SPPs, an external magnetic field is applied to the system, which has the following form:

$$\mathbf{B}(y,t)=\mathbf{e}_x B_0 y, \tag{3}$$

with $B_0$ being the transverse gradient of external field. Then a small but $y$ coordinate dependent Zeeman energy shift is induced to state $|j\rangle$, which reads $\Delta E_j=\mu_B g_F^j m_F^j B_0 y$ ($\mu_B$ is Bohr magneton, $g_F^j$ and $m_F^j$ are gyromagnetic factor and magnetic factor of state $|j\rangle$, respectively). The small energy shift corrects the detuning as $\Delta_j'=\Delta_j-\mu_{j1}B_0 y$, with $\mu_{jl}=\mu_B(g_F^j m_F^j-g_F^l m_F^l)/\hbar$.

In the interaction picture, the simplified Hamiltonian after performing electric-dipole and rotating wave approximations reads

$$\begin{aligned}\hat{H}_{\text{int}}=&-\hbar\sum_{j=2}^{4}\Delta_j'|j\rangle\langle j|-\hbar[\zeta_c(z)e^{i\theta_c}\Omega_c|4\rangle\langle 3|\\&+\zeta_p(z)e^{i\theta_p}\Omega_p|3\rangle\langle 1|+\zeta_s(z)e^{i\theta_s}\Omega_s|3\rangle\langle 1|+\text{H.c.}],\end{aligned} \tag{4}$$

where $\Omega_c=|\mathbf{p}_{34}|\mathcal{E}_c/\hbar$, $\Omega_p=|\mathbf{p}_{13}|\mathcal{E}_p/\hbar$, $\Omega_s=|\mathbf{p}_{23}|\mathcal{E}_s/\hbar$, $\zeta_c(z)=\mathbf{p}_{34}\cdot\mathbf{u}_c(z)/|\mathbf{p}_{34}|$, $\zeta_p(z)=\mathbf{p}_{13}\cdot\mathbf{u}_p(z)/|\mathbf{p}_{13}|$, and $\zeta_s(z)=\mathbf{p}_{23}\cdot\mathbf{u}_s(z)/|\mathbf{p}_{23}|$. Here, $\mathbf{p}_{jl}$ is electric dipole matrix element related to state $|j\rangle$ and state $|l\rangle$, $\theta_c=[k(\omega_c)+k_3-k_4]x$, $\theta_p=[k(\omega_p)+k_1-k_3]x$ and $\theta_s=[k(\omega_c)+k_2-k_3]x$ are the phase mismatch caused by dispersion of SPPs, with $k_l$ ($l=1,\ 2,\ 3,$ and 4) being the wave number of state $|l\rangle$. Note that the Ohmic loss in the system can be characterized by the image part of the phase mismatch, which donates a exponent decay factor of half-Rabi frequency.

The interaction information of the system is given by the density matrix $\sigma$, which is a $4\times4$ matrix. The evolution of $\sigma$ is governed by optical Bloch equation [33]

$$\frac{\partial\sigma}{\partial t}=-\frac{i}{\hbar}[\hat{H}_{\text{int}},\sigma]-\Gamma\sigma, \tag{5}$$

with $\Gamma$ being a $4\times4$ relaxation matrix describing the spontaneous emission and dephasing effect of the system. The explicit expression of Eq. (5) is given in Appendix A.

The evolution of the electric field is given by the Maxwell equations, under slowly varying envelope approximation, the Maxwell equations can be written in form of half-Rabi frequency as follow:

$$\begin{aligned}&i\left(\frac{\partial}{\partial x}+\frac{1}{c}\frac{n^2}{n_{\text{eff}}}\frac{\partial}{\partial t}\right)\Omega_p\zeta_p(z)e^{i\theta_p}+\frac{1}{2k(\omega_p)}\frac{\partial^2}{\partial y^2}\Omega_p\zeta_p(z)e^{i\theta_p}\\&+\kappa_{13}\int_{-\infty}^{\infty}dv f(v)\sigma_{31}=0,\end{aligned} \tag{6a}$$

$$\begin{aligned}&i\left(\frac{\partial}{\partial x}+\frac{1}{c}\frac{n^2}{n_{\text{eff}}}\frac{\partial}{\partial t}\right)\Omega_s\zeta_s(z)e^{i\theta_s}+\frac{1}{2k(\omega_s)}\frac{\partial^2}{\partial y^2}\Omega_s\zeta_s(z)e^{i\theta_s}\\&+\kappa_{23}\int_{-\infty}^{\infty}dv f(v)\sigma_{32}=0,\end{aligned} \tag{6b}$$

where $\kappa_{13}=\mathcal{N}_a|\mathbf{p}_{13}|^2\omega_p^2/[2\varepsilon_0\hbar c^2\tilde{k}(\omega_p)]$, $\kappa_{23}=\mathcal{N}_a|\mathbf{p}_{23}|^2\omega_s^2/[2\varepsilon_0\hbar c^2\tilde{k}(\omega_s)]$ with $\mathcal{N}_a$ the number density of the atoms, $n_{\text{eff}}=k/k_0$ is effective refraction index and $\tilde{k}=\text{Re}(k)$. $v$ is the velocity of the atoms, due to the Doppler effect, the motion of the atoms could cause an inhomogeneous broadening of the energy level, thus, we have averaged Eq. (6) over all atoms weighted by their velocity distribution $f(v)$, which is the Maxwell velocity distribution, and reads [44]

$$f(v)=\frac{\sqrt{\ln 2}}{\sqrt{\pi}W_D}e^{-\ln 2(\frac{kv}{W_D})^2}, \tag{7}$$

where $2W_D=2k\sqrt{2\ln 2k_BT/m_{\text{atom}}}$ is the full width at half maximum (FWHM) of the Doppler broadened line, $T$ is temperature, $k_B$ is the Boltzmann constant, and $m_{\text{atom}}$ is the mass of the atom. The inverted-Y-type four-level system is chosen from hot $^{87}$Rb atomic gas ensemble, and the energy levels are $|1\rangle=|5\,^2S_{1/2},F=1,m_F=-1\rangle$ ($g_F^1=-1/2$), $|2\rangle=|5\,^2S_{1/2},F=1,m_F=1\rangle$ ($g_F^2=-1/2$), $|3\rangle=|5\,^2P_{3/2},F=0,m_F=0\rangle$ ($g_F^3=0$), $|4\rangle=|5\,^2D_{1/2},F=1,m_F=1\rangle$ ($g_F^4=21/10$). Thus, in our case, $\lambda_c\approx\lambda_p\approx\lambda_s=780$ nm, and we can obtain the Doppler width $2W_D=0.55$ GHz.

Equations (5) and (6) are known as the Maxwell-Bloch (MB) equations, which fully describe our system, they can be solved by multiscale method [45]. We take asymptotic expansions of the density matrix elements, the weak probe field and the weaker signal field as: $\sigma_{ij}=\sum_{l=0}^{\infty}\epsilon^l\sigma_{ij}^{(l)}$, $\Omega_p=\sum_{l=1}^{\infty}\epsilon^l\Omega_p^{(l)}$, $\Omega_s=\sum_{l=2}^{\infty}\epsilon^l\Omega_p^{(l)}$, with $\epsilon$ a dimensionless small parameter characterizing the typical amplitude of half-Rabi frequency, $|\Omega_p/\Omega_c|\sim\epsilon$, $|\Omega_s/\Omega_c|\sim\epsilon^2$. In addition, all quantities on the right hand side of expansions are considered as the functions of multiscale variables $x_l=\epsilon^l x(l=0,2)$, $y_1=\epsilon y$, and $t_l=\epsilon^l t(l=0,2)$. In our analysis, the external magnetic field is assumed to be the order of $\epsilon^2$, thus we rewrite the external magnetic field as $B(y)=\epsilon^2B_0y_1$. We substitute the expansions into MB equations, then we will obtain a series of linear but inhomogeneous equations, which can be solved order by order.

## III. LINEAR PROPERTIES AND GAIN ASSISTED PROPAGATION OF SPPs

The zeroth-order approximation of MB equations are acquired by taking $\Omega_p$, $\Omega_s$ and $B(y)$ to be zero (corresponding to the initial state of the system), which reads

$$\sigma_{11}^{(0)}=\frac{\Gamma_{13}}{\Gamma_{41}}\sigma_{33}^{(0)}, \tag{8a}$$

$$\sigma_{22}^{(0)}=\frac{\Gamma_{23}}{\Gamma_{42}}\sigma_{33}^{(0)}, \tag{8b}$$

$$\sigma_{44}^{(0)}=1-\left(\sigma_{11}^{(0)}+\sigma_{22}^{(0)}+\sigma_{33}^{(0)}\right), \tag{8c}$$

$$\sigma_{43}^{(0)}=\frac{\zeta_c(z)\Omega_c}{d_{43}}\left(\sigma_{44}^{(0)}-\sigma_{33}^{(0)}\right), \tag{8d}$$

$$\sigma_{33}^{(0)}=\frac{\Gamma_{41}\Gamma_{42}(2\gamma_{43}|\zeta(z)\Omega_c|^2+\Gamma_{34}|d_{43}|^2)}{\mathcal{J}_1|\zeta_c(z)\Omega_c|^2+\mathcal{J}_2|d_{43}|^2}, \tag{8e}$$

where $\mathcal{J}_1=2\gamma_{43}[\Gamma_{23}\Gamma_{41}+(\Gamma_{13}+2\Gamma_{41})\Gamma_{42}]$, $\mathcal{J}_2=\Gamma_{23}\Gamma_{34}\Gamma_{41}+[\Gamma_{13}\Gamma_{34}+(\Gamma_3+\Gamma_{34})\Gamma_{41}]\Gamma_{42}$, and $\sigma_{21}^{(0)}=\sigma_{31}^{(0)}=$

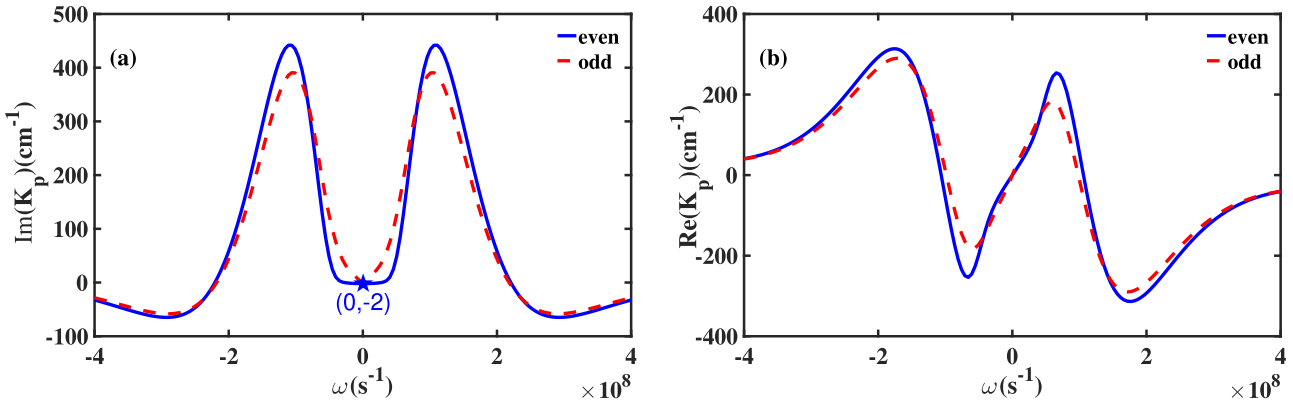


FIG. 2. Linear dispersion relation of the probe field $K_p$ as a function of $\omega$ for different SPPs modes. (a) shows the Im$[K_p(\omega)]$ curves which characterize the linear absorbtion of the system, and (b) shows the Re$[K_p(\omega)]$ curves which characterize the linear dispersion of the system. In both panels, blue solid line is represent for even (symmetric) SPPs mode, while red dashed line for odd (antisymmetric) SPPs mode.

$\sigma_{41}^{(0)} = \sigma_{32}^{(0)} = \sigma_{42}^{(0)} = 0$. $\Gamma_j = \sum_{i<j} \Gamma_{ij}$, and $\gamma_{ij} = (\Gamma_i + \Gamma_j)/2$ donate total spontaneous emission rate of state $|j\rangle$ and dephasing rate of states $|i\rangle$ and $|j\rangle$, respectively. The expression of $\sigma_{33}^{(0)}$ indicates that some atoms will populate in state $|3\rangle$ before probe field and signal field incident into the system, if the incoherent pumping are applied to the system (i.e., $\Gamma_{41} \neq 0, \Gamma_{42} \neq 0$). Thus a Raman-like gain is generated for the probe and signal fields. We can see such a gain effect more clearly in the linear dispersion relation.

In the first- (second-) order approximation of the MB equations, we obtain the solution $\Omega_p^{(1)}(\Omega_s^{(2)})$, $\sigma_{j1}^{(1)}$ $(\sigma_{j2}^{(2)}, j = 3, 4)$, which are proportional to $\exp(i\theta_1)$ $(\exp(i\theta_2))$, with $\theta_1 = K_p(\omega)x_0 - \omega t_0 (\theta_2 = K_s(\omega)x_0 - \omega t_0)$. Here, $K_p(\omega)$, $K_s(\omega)$ are the linear dispersion relation of the probe field and the signal field, which read

$$K_p(\omega) = \frac{\omega}{c}\frac{n^2}{n_{\text{eff}}} + \kappa_{13}\int_{-\infty}^{\infty} dv f(v)\left\langle \frac{D_{11}}{D_1}\right\rangle_z, \tag{9a}$$

$$K_s(\omega) = \frac{\omega}{c}\frac{n^2}{n_{\text{eff}}} + \kappa_{23}\int_{-\infty}^{\infty} dv f(v)\left\langle \frac{D_{21}}{D_2}\right\rangle_z. \tag{9b}$$

We have defined following symbols: $D_1 = (\omega + d_{31}^{(0)})(\omega + d_{41}^{(0)}) - |\zeta(z)\Omega_c|^2$, $D_{11} = (\omega + d_{41}^{(0)})(\sigma_{33}^{(0)} - \sigma_{11}^{(0)}) - \zeta^*(z)\Omega_c^*\sigma_{43}^{(0)}$, $D_2 = (\omega + d_{32}^{(0)})(\omega + d_{42}^{(0)}) - |\zeta(z)\Omega_c|^2$, $D_{21} = (\omega + d_{42}^{(0)})(\sigma_{33}^{(0)} - \sigma_{22}^{(0)}) - \zeta^*(z)\Omega_c^*\sigma_{43}^{(0)}$, and $d_{ij}^{(0)} = \Delta_i - \Delta_j + i\gamma_{ij} (i = 3, 4, j = 1, 2, \Delta_1 = 0)$ is dephasing parameter of zeroth-order approximation. And $\langle g(z)\rangle_z = \int_{-\infty}^{+\infty} g(z)|\zeta(z)|^2 dz / \int_{-\infty}^{+\infty} |\zeta(z)|^2 dz$ donates the expectation value of arbitrary function $g(z)$. Note that in Eqs. (9) and (9b), $\omega$ is the frequency shift to the center frequency of probe and signal field. From Eqs. (9) and (9b), we can find that the mainly difference of the linear dispersion relation $K_p$ and $K_s$ is induced by parameters $\Delta_2$, $\kappa_{j3}$, and $\Gamma_{4j} (j = 1, 2)$. The difference will cause the group velocities mismatch of the probe field and the signal field, thus the probe field could not trap the signal field. In our following analyze, we choose these system parameters as $\Delta_2 = 0$, $\kappa_{13} = \kappa_{23}$ and $\Gamma_{14} = \Gamma_{24}$. Under this condition, the linear dispersion relation of probe field and signal field are almost the same, i.e., $K_p(\omega) \approx K_s(\omega)$, hence the group velocities $(V_{gp(s)} = \text{Re}[\partial K_{p(s)}/\partial\omega]^{-1})$ is well matched.

Figure 2 shows the imaginary part and real part of the linear dispersion relation $K_p(\omega)$ as function of center frequency shift $\omega$. The system parameters are chosen as [44,46]: $|\mathbf{p}_{13}| = |\mathbf{p}_{23}| = 1.46 \times 10^{-29}$ C m, $\Gamma_{13} = \Gamma_{23} = 3$ MHz, $\Gamma_{34} = 1$ MHz, $W_D = 0.28$ GHz. Parameters of the control field and the incoherent pumping are $\Omega_c = 6$ MHz, $\Gamma_{41} = \Gamma_{42} = 2.5$ MHz, respectively. The Detunings are $\Delta_2 = \Delta_3 = \Delta_4 = 0$. In order to obtain a same coupling strength constant, we assume the number density of atoms as $\mathcal{N}_a = 5.84 \times 10^{13}$ cm$^{-3}$ (for symmetric mode), and $\mathcal{N}_a = 1.41 \times 10^{11}$ cm$^{-3}$ (for antisymmetric mode), thus, $\kappa_{13} = \kappa_{23} = 5 \times 10^{11}$ cm$^{-1}$ s$^{-1}$. The parameter of MDM waveguide are: $\mu_1 = \mu_2 = 1$, $\varepsilon_1 = 1$, $\varepsilon_2 = -29.25 + 0.57i$, $d = 300$ nm, and $k = (8.71 + 0.0069i) \times 10^4$ cm$^{-1}$ (for symmetric mode) or $k = (0.021 + 4.91i) \times 10^4$ cm$^{-1}$ (for antisymmetric mode). In Fig. 2, the blue solid line and red dashed line correspond to the even (symmetric) and odd (antisymmetric) SPPs mode.

Figure 2(a) shows the linear absorption spectrum Im$[K_p(\omega)]$. For both symmetric and antisymmetric SPPs modes, the profile of absorption spectrum is a doublet peaks with a transparent window opened at the center frequency $\omega = 0$, which is a EIT phenomenon. Different from usual EIT effect without incoherence pumping, in our system, the transparency window is opened deeply into the region where Im$[K_p(\omega)]$ has a negative value. This means the probe field will obtain a gain from the system, and suppress the Ohmic loss. With the same parameters, the two SPPs modes have similar absorption spectrum as indicates in Fig. 2(a), but the peaks are a bit lower, and the transparency window is slightly narrower and a little deeper for the antisymmetric SPPs mode comparing to the symmetric mode. The difference is mainly due to the slight different field distribution of two SPPs modes.

Figure 2(b) shows the linear dispersion Re$[K_p(\omega)]$. Due to the EIT effect, the dispersion is much enhanced as report in Ref. [32], and we can see that near the resonant point (i.e., $\omega = 0$), Re$[\partial K_p/\partial\omega] > 0$, which means normal dispersion. Further more, in Fig. 2(b), we calculate the group velocity and find that $V_{gp}|_{\omega=0} = 7.72 \times 10^{-6}c$ for antisymmetric mode and $V_{gp}|_{\omega=0} = 1.33 \times 10^{-5}c$ for symmetric mode, both of which correspond to ultra-low group velocity. That indicates we can slow down the group velocity of SPPs in the transparency window. We can also find that there is a region in the transparency

window where satisfies $\mathrm{Re}[\partial K_p/\partial\omega] < 0$, i.e., superluminal group velocity can also be obtained in the system for the two SPPs modes.

Note that the gain assisted propagation of SPPs in our system and group velocity match condition is significant important in our following analyze. Also, we will mainly focus on the symmetry SPPs mode in our following analyze due to the antisymmetry mode has a large Ohmic loss ($\mathrm{Im}(k) \gg 0$).

## IV. NONLINEAR EVOLUTION EQUATION OF SPPs SOLITON

In this section, we will derive the nonlinear evolution equation of the probe field and the signal field. In previous section, we give the solution of the MB equations up to second-order approximation, and the density matrix element $\sigma_{ij}^{(l)}(l = 0, 1, 2)$ is obtained but with two unknown function to be determined. The explicit expression of $\sigma_{ij}^{(l)}(l = 1, 2)$ is available in Appendix B. The unknown functions are the envelope functions of the probe field and the signal field, which satisfy $\Omega_p^{(1)} = F_p \exp(i\theta_1)$ and $\Omega_s^{(2)} = F_s \exp(i\theta_2)$. $F_p$ and $F_s$ are function of multiscale variables. Substitute the gotten solution into the third-order approximation equations, we got the solvable condition of $F_p$

$$i\left(\frac{\partial}{\partial x_2} + \frac{1}{V_{gp}}\frac{\partial}{\partial t_2}\right)F_p + \frac{1}{2k_p}\frac{\partial^2}{\partial y_2^2}F_p - W_{pp}|F_p|^2F_p e^{-2\bar{\alpha}_p x_2} + B_0 M_p \cdot y_1 F_p = 0, \tag{10}$$

with $\bar{\alpha}_p = \alpha_p/\epsilon^2$, $\alpha_p = \mathrm{Im}(k + K_p)$, coefficient $W_{pp}$ and $M_p$ are given in Appendix B.

Similarly, we obtain the solvable condition of $F_s$ in the fourth-order approximation.

$$i\left(\frac{\partial}{\partial x_2} + \frac{1}{V_{gs}}\frac{\partial}{\partial t_2}\right)F_s + \frac{1}{2k_s}\frac{\partial^2}{\partial y_2^2}F_s - W_{sp}|F_p|^2F_s e^{(-2\bar{\alpha}_p x_2)} + B_0 M_s \cdot y_1 F_s = 0, \tag{11}$$

and coefficient $W_{sp}$ and $M_s$ are given in Appendix B.

Combining each order solution and returning to the original variable scale $(x, y, t)$, Eqs. (10) and (11) can be written in dimensionless form

$$\frac{i}{\lambda}\frac{\partial u_p}{\partial\tau} + \frac{1}{2}\frac{\partial^2 u_p}{\partial\xi^2} - w_p|u_p|^2u_p + \mathcal{M}_p\xi u_p = -ia_p u_p, \tag{12a}$$

$$\frac{i}{\lambda}\frac{\partial u_s}{\partial\tau} + \frac{1}{2}\frac{\partial^2 u_s}{\partial\xi^2} - w_s|u_p|^2u_s + \mathcal{M}_s\xi u_s = -ia_s u_s, \tag{12b}$$

where the dimensionless variables are defined as $\eta = (x - V_{gp}t)/L_{\mathrm{Diff}}$, $\xi = y/R_y$, $\tau = t/\tau_0$ and $u_j = u_j(\eta, \xi, \tau) = \Omega_j \exp[-i\mathrm{Re}(K_j|_{\omega=0})x]/U_0 (j = p, s)$. Here, $L_{\mathrm{Diff}} = kR_y^2$, $R_y$, $\tau_0$ and $U_0$ are typical scale quantities characterizing typical diffraction length, waist radius of incident laser beam, probe-pulse duration and typical half-Rabi frequency, respectively. And $w_j = W_{jp}/|W_{pp}| (j = s, p)$ is coefficient characterizing self-phase ($w_p$) or cross-phase ($w_s$) modulation, $a_j = \mathrm{Im}(k + K_j|_{\omega=0})\, L_{\mathrm{Diff}} (j = s, p)$ characterizes the absorption, $\lambda = V_{gp}\tau_0/L_{\mathrm{Diff}}$ is dimensionless group velocity, $\mathcal{M}_j = B_0 M_j R_y^2 L_{\mathrm{Diff}} (j = s, p)$.

One can find that the derivative in variable $\eta$ is not apparent in Eq. (12), thus the variable $\eta$ is separable from $u_j$, i.e., $u_j(\eta, \xi, \tau) = f_j(\eta) \cdot v_j(\xi, \tau)$. Note that $\eta$ is a local variable associated to a frame moving in $x-$ direction with velocity $V_{gp}$, which means the envelope of probe and signal field is shape-preserved in the $x$ direction with profile $f_j(x/L_{\mathrm{Diff}})$. Without loss of generality, we assume $f_j$ has a Gauss profile: $f_j(\eta) = \exp(-\eta^2/2\rho_0^2)/\sqrt{2\pi\rho_0^2}$ and $\int_{-\infty}^{+\infty}|f_j(\eta)|^2 d\eta = 1$ is satisfied. During above derivation, we have used the group velocity match condition.

After integrating the Eq. (12) over variable $\eta$, then we obtain

$$\frac{i}{\lambda}\frac{\partial v_p}{\partial\tau} + \frac{1}{2}\frac{\partial^2 v_p}{\partial\xi^2} - w_p|v_p|^2v_p + \mathcal{M}_p\xi v_p = 0, \tag{13a}$$

$$\frac{i}{\lambda}\frac{\partial v_s}{\partial\tau} + \frac{1}{2}\frac{\partial^2 v_s}{\partial\xi^2} - w_s|v_p|^2v_s + \mathcal{M}_s\xi v_s = 0. \tag{13b}$$

We have neglected the absorption term $(-ia_j)$ in Eq. (12). This is valid with the gain induced by the incoherent pumping. Equation (13) is the system equation which describes the nonlinear evolution of the probe field and the signal field. Generally speaking, Eq. (13) is not always integrable due to the coefficients $\lambda$, $w_j$ and $\mathcal{M}_j$ are complex number. However, we will show later that we can choose a set of realistic physical parameters to make all these coefficients have a much smaller imaginary part than their corresponding real part. Thus, it is possible to get shape preserving solution from Eq. (13), i.e., SPPs soliton is available in the system.

## V. CONTROLLING SIGNAL SPPs SOLITON WITH PROBE SPPs SOLITON VIA CROSS-PHASE MODULATION

We now investigate the manipulation of the low-loss SPPs soliton in MDM waveguide system. To obtain a shape-preserved SPPs, the realistic physical parameters are chosen as following for symmetric mode: $\Omega_c = 0.2$ GHz, $\Gamma_{41} = \Gamma_{42} = 15.5$ MHz, $\Delta_2 = 0$, $\Delta_3 = 71.43$ MHz, $\Delta_4 = 0.1$ MHz, and $\tau_0$, $R_y$ and other system parameters are the same as that we used in antisymmetric case. And we obtain $L_{\mathrm{Diff}} = 0.087$ cm, $M_p = (-9.77 - 0.50i) \times 10^5\ \mathrm{cm^{-1}\,T^{-1}}$, $M_s = (-1.58 - 0.085i) \times 10^6\ \mathrm{cm^{-1}\,T^{-1}}$, the corresponding dimensionless coefficients are $\lambda = -0.99 + 0.057i$, $w_p \approx w_s = -0.99 - 0.13i$, $a_p \approx a_s = 0.0018$. We can see that for both the antisymmetric and symmetric SPPs modes, the corresponding system parameters can make sure the imaginary parts of dimensionless coefficients much smaller than their corresponding real parts, and the absorbtion term $a_p(a_s)$ can be neglected.

### A. Manipulate signal SPPs without external magnetic field

We firstly consider the case when the external magnetic field is absent, i.e., $B_0 = 0$ (thus $\mathcal{M}_s = \mathcal{M}_p = 0$). In this case, the evolution equation of the probe field Eq. (13) is a nonlinear Schrödinger equation (NLSE), and it has single soliton solution [31,32]. What we are more interested is the evolution of the signal SPPs. From Eq. (13b), we know that the evolution of the signal SPPs ($v_s$) is coupled to the probe SPPs ($v_p$), which is known as cross-phase modulation (CPM)

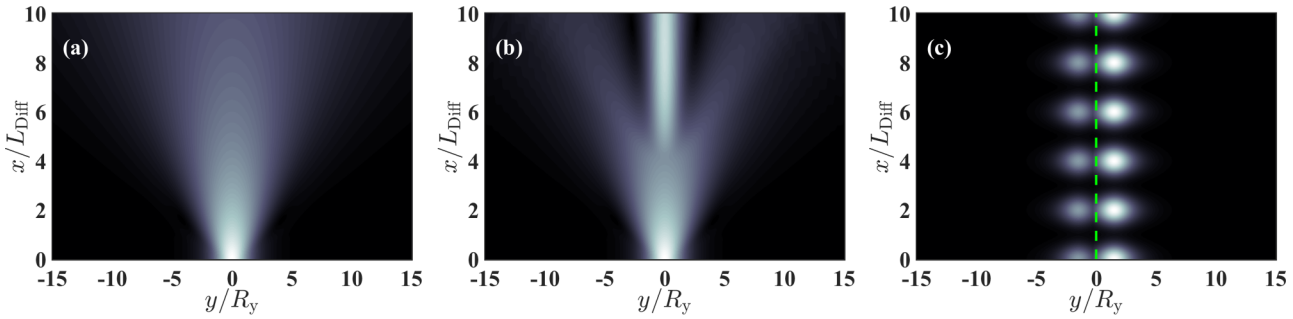


FIG. 3. Propagation of the signal SPPs (a) without and (b) and (c) with the probe SPPs. In (a), the signal SPPs diffused quickly due to the diffraction effect. In (b), the probe SPPs is excited when the signal SPPs propagates to $x = 4L_{\mathrm{Diff}}$, and the signal SPPs is firstly diffused, then focused and maintain its shape. In (c), both signal (weaker) and probe SPPs are excited at $x = 0$, and the signal SPPs is trapped by the probe SPPs without diffusion, and the green dotted line is the trajectory of the SPPs pulse center. The Gaussian profile of SPPs in the $x$ direction is used only in (c).

[40,41], and is characterized by coefficient $w_{21}$ ($W_{21}$). We can control the propagation of the signal SPPs via modulating CPM. Figure 3 shows the numerical result of Eq. (13), and the initial profile of the signal SPPs is $v_s(\xi, 0) = 0.2\mathrm{sech}(\xi)$. In Fig. 3(a), the probe SPPs is absent, thus there is no CPM, and with the propagation distance increasing the signal SPPs diffuses rapidly due to the diffraction effect.

In Fig. 3(b), the input signal SPPs has the same profile as that in Fig. 3(a), but a probe SPPs is excited as the signal SPPs propagates to the position $x = 4L_{\mathrm{Diff}}$. The initial profile of the probe SPPs reads $v_p(\xi, 4/\lambda) = \mathrm{sech}(\xi)$, which has the same pulse width as signal's but a lager amplitude. Before the probe SPPs is excited, there is no CPM and signal diffuses. Then as the probe SPPs excited, the central part of diffused signal SPPs is focused, and its shape is preserved in the later evolution. That means the diffused signal SPPs could be refocused via CPM. As discussed in former section, the CPM can work continuously thanks to the group velocity matched.

Note that in both Figs. 3(a) and 3(b), we have set $f_j(\eta) = 1$ to observe the diffraction effect intuitively. However, in Fig. 3(c), $f_j(\eta)$ is taken as the Gaussian profile we mentioned in former section. And the probe and signal SPPs are launched together with initial pulses $v_p = \mathrm{sech}(\xi)$ and $v_s = 0.2\mathrm{sech}(\xi)$. From Eq. (13) we know that the weak signal would not affect the evolution of probe SPPs, and the numerical result in Fig. 3(c) shows that the probe SPPs (brighter spot in the figure) propagates along the $x$ direction directly. Due to the CPM and group velocity matched condition, the signal SPPs (darker spot in the figure, its amplitude is multiplied by 3 in the figure due to its intensity is much weak than probe field) is carried by the probe SPPs, and maintains its shape to distance. The numerical result indicates the weak signal SPPs is trapped by the probe SPPs, and the CPM provide a enough nonlinearity for the signal SPPs to balance the diffraction effect. Note that in this article, the green dotted line in all figures is the central trajectory of the two SPPs, and we have dislocated the center of the SPPs into the two side of the trajectory to show the trapping effect.

The CPM effect in the system not only can be used to focus and trap the weak signal SPPs but also provide a method to reshape the weak signal SPPs. Shown in Fig. 4 is the intensity distribution of the signal SPPs ($|\Omega_s/U_0|$) during its evolution ($f_j(\eta) = 1$ for intuitive). Panel (a) and panel (b) are numerically simulated with the same initial signal SPPs pulse $v_s = 0.1\mathrm{sech}(\xi)$ but different initial probe SPPs pulse: $v_p = \mathrm{sech}(\xi)$ (basic state solition) for panel(a) and $v_p = 2\mathrm{sech}(\xi)$ (first-order soliton) for panel (b). As illustrated in Fig. 4, the signal SPPs evolutes to a basic soliton when the input probe SPPs is a basic soliton [panel (a)] or evolute to a first-order soliton when the input probe SPPs is a first-order soliton [panel (b)]. In other words, when the signal SPPs is trapped by the probe SPPs, the signal SPPs will follow the probe SPPs's evolution due to CPM.

### B. Manipulate signal SPPs with external magnetic field

We now consider the influence of the external magnetic field to the system. When the external magnetic field applied to the system, $\mathcal{M}_p \neq 0$ and $\mathcal{M}_s \neq 0$ (due to $B_0 \neq 0$). Then Eq. (13) is a NLSE with external potential, and Eq. (13b) remains the same as that in the case of last subsection. Using quasiparticle theory [47,48], a shape preserved solution of Eq. (13) is still available but the solution with a transverse movement due to the external potential, which is induced by the external magnetic field with transverse gradient. However, the solution of the signal SPPs can not equally feel the external potential as the probe SPPs does in our system (due to $\mathcal{M}_s \neq \mathcal{M}_p$). Thus, to trap signal SPPs efficiently, a stronger CPM is need, which means the probe SPPs pulse should have a larger pulse amplitude as well as narrower pulse width in space. We simulate the trapping effect when the magnetic field is applied to the system as shown in Fig. 5.

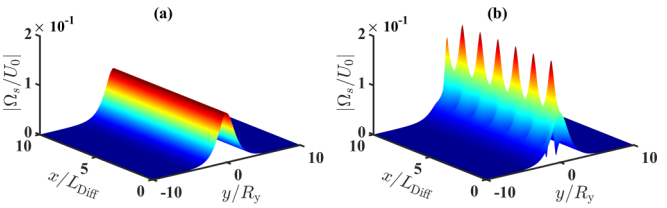


FIG. 4. Propagation of the signal SPPs (a) when the signal SPPs is trapped by the probe SPPs with initial shape $v_p = \mathrm{sech}(\xi)$ and (b) when the signal SPPs is trapped by the probe SPPs with initial shape $v_p = 2\mathrm{sech}(\xi)$. In both panels, the initial shape of the signal SPPs is $v_s = 0.1\mathrm{sech}(\xi)$.

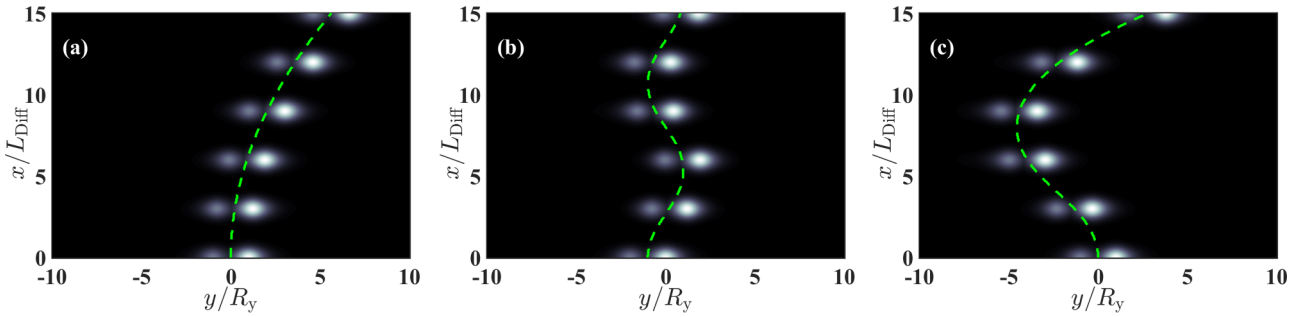


FIG. 5. Dynamic trapping and trajectory control of the signal SPPs. (a) The signal SPPs trapped by the probe SPPs and deflects in the $y$ direction with an external magnetic field $\mathbf{B} = B_0 y \mathbf{e}_x$. (b) The signal SPPs trapped by the probe SPPs and oscillates in the $y$ direction with an external magnetic field $\mathbf{B} = B_0 \tanh(y)\, y \mathbf{e}_x$. (c) The signal SPPs trapped by the probe SPPs and deflects in the $y$ direction with a time-dependent external magnetic field $\mathbf{B} = B_0 \tanh(t - t_0) y \mathbf{e}_x$. In all panels, the green dotted line is the trajectory of the SPPs pulse center, and the brighter spot represents the probe SPPs and the darker spot represents the signal SPPs.

Figure 5(a) shows the trapping effect when the magnetic field is $\mathbf{B} = B_0 y \mathbf{e}_x$ with $B_0 = 5.88 \times 10^{-4}\ \mathrm{T\,cm^{-1}}$, with the initial probe SPPs pulse $v_p = 2\mathrm{sech}(2\xi)$ and the initial signal SPPs pulse $v_s = 0.2\mathrm{sech}(2\xi)$. It is obvious that the probe SPPs is deflect in the $y$ direction, while signal SPPs is trapped and deflect simultaneously as the probe SPPs. From Eq. (13), we know that the trajectory (green dotted line) of the SPPs is parabola. With different magnetic field gradient $B_0$, we can obtain different parabola trajectory of SPPs, and can carry weak signal SPPs to output at different positions.

We can also make the SPPs to oscillate in the $y$ direction during the propagation of SPPs. Figure 5(b) is the evolution of SPPs when the external magnetic field has a symmetric gradient about $y = 0$ which reads $\mathbf{B} = B_0 \tanh(y) y \mathbf{e}_x$ with $B_0 = 3.50 \times 10^{-3}\ \mathrm{T\,cm^{-1}}$, the initial SPPs pulses $v_p = 2\mathrm{sech}[2(\xi + 1)]$, $v_s = 0.2\mathrm{sech}[2(\xi + 1)]$. In this case, the probe SPPs carries the signal SPPs and oscillate in the $y$ direction around $y = 0$ like a classical partial trapped in a potential well. Using such a method, we can bind the SPPs to propagate in a finite space in the $y$ direction.

The trapping effect is still effective when the magnetic field is time-dependent. Fig. 5(c) is the numerical result when the magnetic field takes the form $\mathbf{B} = B_0 \tanh(t - t_0) y \mathbf{e}_x$ and $B_0 = 3.50 \times 10^{-3}\ \mathrm{T\,cm^{-1}}$, $t_0 = 4|\lambda\tau_0|$, the initial SPPs pulse profile are the same as that in panel(a). In such a magnetic field, the trajectory of SPPs is complicated but a dynamic trapping of the signal SPPs is realized. Note that the intensity(amplitude of signal field) of all dark spots in Fig. 5 is 5 times larger than its real value for intuitive.

## VI. CONCLUSION

In conclusion, a scheme based on EIT with incoherent pumping is proposed to support the low-loss propagation of the SPPs in the MDM waveguide for both symmetric and antisymmetric modes, and further more, the trapping effect and trajectory control of the SPPs is realized via CPM and the external gradient magnetic field. We found the lossy SPPs in the MDM waveguide can acquire a gain to counteract the absorption using incoherent pumping. We also shown that both subluminal and superluminal SPPs are available in our system. Our system also support the SPPs soliton solutions, and a weak and diffused signal SPPs can be trapped by the probe SPPs via CPM, thus, the weak signal SPPs can be carried to a distent position without much diffuse. Our results reveal that the trapping effect can be used to focus a diffused SPPs, and the trapped signal SPPs has a similar evolution as the probe SPPs, thus we can use this method to reshape the weak signal SPPs via changing the shape of probe SPPs. We further prove that a external gradient magnetic field can deflect the probe SPPs in our system, and the weak signal SPPs could still be trapped by probe SPPs. By carefully designing the magnetic gradient, a complicated trajectory can be obtained, and we can realize the dynamic trajectory control of the SPPs.

The scheme we proposed is more general than that in free space, and the results obtained of our work are helpful for understanding the nonlinear features in the interaction between SPPs with coherent mediums, and also have potential applications in micro/nano-optics such as in future on-cheap optical circuit, quantum information processing, etc.

## ACKNOWLEDGMENTS

This work was supported by National Natural Science Foundation of China (NSFC) under Grants No. 11604185 and No. 11804196, the Taishan Scholar Program of Shandong Province of China.

## APPENDIX A: THE BLOCH EQUATIONS

The explicit Bloch equations in terms of density matrix elements are given by

$$i\frac{\partial \sigma_{11}}{\partial t} + i\Gamma_{41}\sigma_{11} - i\Gamma_{13}\sigma_{33} + e^{-i\theta_p^*}\zeta^*(z)\Omega_p^*\sigma_{31} - e^{i\theta_p}\zeta(z)\Omega_p\sigma_{31}^* = 0, \tag{A1a}$$

$$i\frac{\partial \sigma_{22}}{\partial t} + i\Gamma_{42}\sigma_{22} - i\Gamma_{23}\sigma_{33} + e^{-i\theta_s^*}\zeta^*(z)\Omega_s^*\sigma_{32} - e^{i\theta_s}\zeta(z)\Omega_s\sigma_{32}^* = 0, \tag{A1b}$$

$$i\frac{\partial\sigma_{33}}{\partial t}+i\Gamma_3\sigma_{33}-i\Gamma_{34}\sigma_{44}+[\zeta^*(z)\Omega_c^*\sigma_{43}+e^{i\theta_p}\zeta(z)\Omega_p\sigma_{31}^*+e^{i\theta_s}\zeta(z)\Omega_s\sigma_{32}^*-\text{c.c.}]=0, \tag{A1c}$$

$$i\frac{\partial\sigma_{44}}{\partial t}+i\Gamma_{34}\sigma_{44}-i\Gamma_{41}\sigma_{11}-i\Gamma_{42}\sigma_{22}+\zeta(z)\Omega_c\sigma_{43}^*-\zeta^*(z)\Omega_c^*\sigma_{43}=0, \tag{A1d}$$

$$\left(i\frac{\partial}{\partial t}+d_{21}\right)\sigma_{21}+e^{-i\theta_s^*}\zeta^*(z)\Omega_s^*\sigma_{31}-e^{i\theta_p}\zeta(z)\Omega_p\sigma_{32}^*=0, \tag{A1e}$$

$$\left(i\frac{\partial}{\partial t}+d_{31}\right)\sigma_{31}+\zeta^*(z)\Omega_c^*\sigma_{41}+e^{i\theta_p}\zeta(z)\Omega_p(\sigma_{11}-\sigma_{33})+e^{i\theta_s}\zeta(z)\Omega_s\sigma_{21}=0, \tag{A1f}$$

$$\left(i\frac{\partial}{\partial t}+d_{32}\right)\sigma_{32}+\zeta^*(z)\Omega_c^*\sigma_{42}+e^{i\theta_p}\zeta(z)\Omega_p\sigma_{21}^*+e^{i\theta_s}\zeta(z)\Omega_s(\sigma_{22}-\sigma_{33})=0, \tag{A1g}$$

$$\left(i\frac{\partial}{\partial t}+d_{41}\right)\sigma_{41}+\zeta(z)\Omega_c\sigma_{31}-e^{i\theta_p}\zeta(z)\Omega_p\sigma_{43}=0, \tag{A1h}$$

$$\left(i\frac{\partial}{\partial t}+d_{42}\right)\sigma_{42}+\zeta(z)\Omega_c\sigma_{32}-e^{i\theta_s}\zeta(z)\Omega_s\sigma_{43}=0, \tag{A1i}$$

$$\left(i\frac{\partial}{\partial t}+d_{43}\right)\sigma_{43}+\zeta(z)\Omega_c(\sigma_{33}-\sigma_{44})-e^{-i\theta_p^*}\zeta^*(z)\Omega_p^*\sigma_{41}-e^{-i\theta_s^*}\zeta^*(z)\Omega_s^*\sigma_{42}=0, \tag{A1j}$$

where $d_{21}=-[\mathbf{k}(\omega_p)-\mathbf{k}(\omega_p)]\cdot\mathbf{v}+\Delta_2'+i\gamma_{21}$, $d_{31}=-\mathbf{k}(\omega_p)\cdot\mathbf{v}+\Delta_3'+i\gamma_{31}$, $d_{32}=-\mathbf{k}(\omega_s)\cdot\mathbf{v}+\Delta_3'-\Delta_2'+i\gamma_{32}$, $d_{41}=-[\mathbf{k}(\omega_c)+\mathbf{k}(\omega_p)]\cdot\mathbf{v}+\Delta_4'+i\gamma_{41}$, $d_{42}=-[\mathbf{k}(\omega_c)+\mathbf{k}(\omega_s)]\cdot\mathbf{v}+\Delta_4'-\Delta_2'+i\gamma_{42}$, $d_{43}=-\mathbf{k}(\omega_c)\cdot\mathbf{v}+\Delta_4'-\Delta_3'+i\gamma_{43}$, $\mathbf{v}$ is the velocity of the atoms, and satisfies the Maxwell distribution function. We can see that compare to the case in free space, the Bloch equations in waveguide system have additional coefficient $\exp(i\theta_l)(l=c,p,s)$ accompany with half-Rabi frequency $\Omega_l(l=c,p,s)$ due to the phase match, also contains the Ohmic loss. Given that the half-Rabi frequency of control field ($\Omega_c$) is strong enough in our system, the coefficient $\exp(i\theta_c)$ is neglected in the above equations.

## APPENDIX B: SOLUTIONS OF THE BLOCH EQUATIONS

The Bloch equations are solved by using the multiscale method, the solution of density matrix element $\sigma_{ij}=\sigma_{ij}^{(0)}+\epsilon\sigma_{ij}^{(1)}+\epsilon^2\sigma_{ij}^{(2)}+\epsilon^3\sigma_{ij}^{(3)}+\ldots$, and the solution $\sigma_{ij}^{(k)}(k=1,2,3)$ are given as following.

### 1. The first-order approximation

$$\Omega_p^{(1)}=F_p\,\exp(i\theta_1), \tag{B1a}$$

$$\sigma_{31}^{(1)}=\zeta(z)\frac{D_{11}}{D_1}F_p\,\exp[i(\theta_1+\theta_p)], \tag{B1b}$$

$$\sigma_{41}^{(1)}=\zeta(z)\frac{D_{12}}{D_1}F_p\,\exp[i(\theta_1+\theta_p)], \tag{B1c}$$

where $D_{12}=(\omega+d_{31}^{(0)})\sigma_{43}^{(0)}-\zeta(z)\Omega_c(\sigma_{33}^{(0)}-\sigma_{11}^{(0)})$. And $\sigma_{21}^{(1)}=\sigma_{32}^{(1)}=\sigma_{42}^{(1)}=\sigma_{43}^{(1)}=\sigma_{jj}^{(1)}\equiv 0(j=1-4)$, $\Omega_s^{(1)}=0$.

### 2. The second-order approximation

$$\Omega_s^{(1)}=F_s\,\exp(i\theta_2), \tag{B2a}$$

$$\sigma_{32}^{(1)}=\zeta(z)\frac{D_{21}}{D_2}F_s\,\exp[i(\theta_2+\theta_s)], \tag{B2b}$$

$$\sigma_{42}^{(1)}=\zeta(z)\frac{D_{22}}{D_2}F_s\,\exp[i(\theta_2+\theta_s)], \tag{B2c}$$

$$\sigma_{11}^{(2)}=a_{11}|F_p|^2|\zeta(z)|^2e^{-2\bar{\alpha}_px_2}, \tag{B2d}$$

$$\sigma_{22}^{(2)}=a_{22}|F_p|^2|\zeta(z)|^2e^{-2\bar{\alpha}_px_2}, \tag{B2e}$$

$$\sigma_{33}^{(2)}=a_{33}|F_p|^2|\zeta(z)|^2e^{-2\bar{\alpha}_px_2}, \tag{B2f}$$

$$\sigma_{44}^{(2)}=a_{44}|F_p|^2|\zeta(z)|^2e^{-2\bar{\alpha}_px_2}, \tag{B2g}$$

$$\sigma_{43}^{(2)}=a_{43}|F_p|^2|\zeta(z)|^2e^{-2\bar{\alpha}_px_2}, \tag{B2h}$$

where $D_{22} = (\omega + d_{32}^{(0)})\sigma_{43}^{(0)} - \zeta(z)\Omega_c(\sigma_{33}^{(0)} - \sigma_{22}^{(0)})$, $a_{11} = (a_1 + a_2\sigma_{11}^{(0)})$, $a_{22} = a_2\sigma_{22}^{(0)}$, $a_{33} = a_2\sigma_{33}^{(0)}$, $a_{44} = (a_2\sigma_{44}^{(0)} - a_1 - a_2)$, with

$$a_1 = \frac{i}{\Gamma_{41}}\left(\frac{D_{11}}{D_1} - \frac{D_{11}^*}{D_1^*}\right),$$

$$a_2 = \left[\frac{1}{2\gamma_{43}|\zeta(z)\Omega_c|^2 + \Gamma_{34}\left|d_{43}^{(0)}\right|^2}\left(\frac{id_{43}^{*(0)}\zeta^*(z)\Omega_c^* D_{12}}{D_1} - \frac{id_{43}^{(0)}\zeta(z)\Omega_c D_{12}^*}{D_1^*}\right) - a_1\left(\frac{\Gamma_{41}\left|d_{43}^{(0)}\right|^2}{2\gamma_{43}|\zeta(z)\Omega_c|^2 + \Gamma_{34}\left|d_{43}^{(0)}\right|^2} + 1\right)\right],$$

$$a_{43} = \frac{1}{d_{43}^{(0)}}\left[\frac{D_{12}}{D_1} + \zeta(z)\Omega_c(a_{44} - a_{33})\right],$$

and $\sigma_{21}^{(2)} = \sigma_{31}^{(2)} = \sigma_{41}^{(2)} \equiv 0$, $\Omega_p^{(2)} = 0$.

### 3. The third-order approximation

$$\sigma_{21}^{(3)} = a_{21}^{(3)}F_pF_s^*|\zeta(z)|^2\zeta(z)e^{i(\theta_1 - \theta_2^* + \theta_p - \theta_s^*)}, \tag{B3a}$$

$$\sigma_{31}^{(3)} = \left(a_{31,1}^{(3)}|F_p|^2F_p|\zeta(z)|^2e^{-2\bar{\alpha}_p x_2} + a_{31,2}^{(3)}\partial_{t_2}F_p + a_{31,3}^{(3)}F_p\right)\zeta(z)e^{i(\theta_1+\theta_p)}, \tag{B3b}$$

$$\sigma_{41}^{(3)} = \left(a_{41,1}^{(3)}|F_p|^2F_p|\zeta(z)|^2e^{-2\bar{\alpha}_p x_2} + a_{41,2}^{(3)}\partial_{t_2}F_p + a_{41,3}^{(3)}F_p\right)\zeta(z)e^{i(\theta_1+\theta_p)}, \tag{B3c}$$

with the coefficients

$$a_{21}^{(3)} = \frac{1}{\omega + d_{21}^{(0)}}\left(\frac{D_{21}^*}{D_2^*} - \frac{D_{11}}{D_1}\right),$$

$$a_{31,1}^{(3)} = \frac{(a_{33} - a_{11})\left(\omega + d_{41}^{(0)}\right) - a_{43}\zeta^*(z)\Omega_c^*}{D_1},$$

$$a_{31,2}^{(3)} = -i\frac{D_{11}\left(\omega + d_{41}^{(0)}\right) - D_{12}\zeta^*(z)\Omega_c^*}{D_1^2},$$

$$a_{31,3}^{(3)} = \frac{d_{41}^{(2)}D_{12}\zeta^*(z)\Omega_c^* - d_{31}^{(2)}D_{11}\left(\omega + d_{41}^{(0)}\right)}{D_1^2},$$

$$a_{41,1}^{(3)} = \frac{(a_{11} - a_{33})\zeta(z)\Omega_c + a_{43}(\omega + d_{31})}{D_1},$$

$$a_{41,2}^{(3)} = i\frac{D_{11}\zeta(z)\Omega_c - D_{12}\left(\omega + d_{31}^{(0)}\right)}{D_1^2},$$

$$a_{41,3}^{(3)} = \frac{d_{31}^{(2)}D_{11}\zeta(z)\Omega_c - d_{41}^{(2)}D_{12}\left(\omega + d_{31}^{(0)}\right)}{D_1^2},$$

with $d_{ij}^{(2)} = -B_0y_1\,\mu_{ij}$. Others elements in the third approximation are all equal to zero. We also obtain the coefficient in Eq. (10)

$$W_{11} = \kappa_{13}\int_{-\infty}^{\infty}dvf(v)\left\langle|\zeta(z)|^2\frac{a_{43}\Omega_c^* + (a_{11} - a_{33})\left(\omega + d_{41}^{(0)}\right)}{D_1}\right\rangle_z, \tag{B4}$$

$$M_p = \kappa_{13}\int_{-\infty}^{\infty}dvf(v)\left\langle\frac{\mu_{31}D_{11}\left(\omega + d_{41}^{(0)}\right) - \mu_{41}D_{12}\Omega_c^*}{D_1^2}\right\rangle_z. \tag{B5}$$

### 4. The fourth-order approximation

In the fourth-order approximation, we obtain the coefficient in Eq. (11)

$$W_{21} = \kappa_{23}\int_{-\infty}^{\infty}dvf(v)\left\langle|\zeta(z)|^2\frac{a_{43}\Omega_c^* + \left(a_{21}^{(3)*} + a_{22} - a_{33}\right)\left(\omega + d_{42}^{(0)}\right)}{D_2}\right\rangle_z, \tag{B6}$$

$$M_s = \kappa_{23}\int_{-\infty}^{\infty}dvf(v)\left\langle\frac{\mu_{32}D_{21}\left(\omega + d_{42}^{(0)}\right) - \mu_{42}D_{22}\Omega_c^*}{D_2^2}\right\rangle_z. \tag{B7}$$

[1] Y. Fang and M. Sun, Light-Sci. Appl. **4**, e294 (2015).
[2] K. MacDonald and N. Zheludev, Laser Photon. Rev. **4**, 562 (2010).
[3] C. Karnetzky, P. Zimmermann, C. Trummer, C. D. Sierra, M. Wörle, R. Kienberger, and A. Holleitner, Nat. Commun. **9**, 2471 (2018).
[4] J. Wang, L. Zhao, Z.-C. Hao, X. Shen, and T. J. Cui, Opt. Lett. **44**, 3374 (2019).
[5] Y. Fu, X. Hu, C. Lu, S. Yue, H. Yang, and Q. Gong, Nano Lett. **12**, 5784 (2012).
[6] M. S. Tame, K. R. McEnery, S. K. Özdemir, J. Lee, S. A. Maier, and M. S. Kim, Nat. Phys. **9**, 329 (2013).
[7] N. Jiang, X. Zhuo, and J. Wang, Chem. Rev. **118**, 3054 (2018).
[8] J. S. Pae, S. J. Im, K. S. Ho, C. S. Ri, S. B. Ro, and J. Herrmann, Phys. Rev. B **98**, 041406(R) (2018).
[9] K. S. Ho, S. J. Im, J. S. Pae, C. S. Ri, Y. H. Han, and J. Herrmann, Sci. Rep. **8**, 10584 (2018).
[10] J. Gosciniak, S. I. Bozhevolnyi, T. B. Andersen, V. S. Volkov, J. Kjelstrup-Hansen, L. Markey, and A. Dereux, Opt. Express **18**, 1207 (2010).
[11] M. J. Dicken, L. A. Sweatlock, D. Pacifici, H. J. Lezec, K. Bhattacharya, and H. A. Atwater, Nano Lett. **8**, 4048 (2008).
[12] L. Liu, L. Kang, T. S. Mayer, and D. H. Werner, Nat. Commun. **7**, 13236 (2016).
[13] V. V. Temnov, Nat. Photonics **6**, 728 (2012).
[14] W. F. Zhang, X. Zhang, Y. V. Kartashov, X. Chen, and F. Ye, Phys. Rev. A **97**, 063845 (2018).
[15] A. Block, C. Etrich, T. Limboeck, F. Bleckmann, E. Soergel, C. Rockstuhl, and S. Linden, Nat. Commun. **5**, 3843 (2014).
[16] B. Gjonaj, J. Aulbach, P. M. Johnson, A. P. Mosk, L. Kuipers, and A. Lagendijk, Nat. Photonics **5**, 360 (2011).
[17] J. Lin, J. B. Mueller, Q. Wang, G. Yuan, N. Antoniou, X. C. Yuan, and F. Capasso, Science **340**, 331 (2013).
[18] C. Du, Q. Jing, and Z. Hu, Phys. Rev. A **91**, 013817 (2015).
[19] C. F. Kuo and S. C. Chu, Opt. Express **26**, 19123 (2018).
[20] A. Salandrino and D. N. Christodoulides, Opt. Lett. **35**, 2082 (2010).
[21] N. K. Efremidis, Z. Chen, M. Segev, and D. N. Christodoulides, Optica **6**, 686 (2019).
[22] P. Zhang, Y. Hu, T. Li, D. Cannan, X. Yin, R. Morandotti, Z. Chen, and X. Zhang, Phys. Rev. Lett. **109**, 193901 (2012).
[23] I. Epstein and A. Arie, Phys. Rev. Lett. **112**, 023903 (2014).
[24] S. Wang, S. Wang, and Y. Zhang, Opt. Express **26**, 5461 (2018).
[25] M. Fleischhauer, A. Imamoglu, and J. P. Marangos, Rev. Mod. Phys. **77**, 633 (2005).
[26] N. Khan, B. Amin Bacha, A. Iqbal, A. Ur Rahman, and A. Afaq, Phys. Rev. A **96**, 013848 (2017).
[27] A. Kamli, S. A. Moiseev, and B. C. Sanders, Phys. Rev. Lett. **101**, 263601 (2008).
[28] S. A. Moiseev, A. A. Kamli, and B. C. Sanders, Phys. Rev. A **81**, 033839 (2010).
[29] M. Siomau, A. A. Kamli, S. A. Moiseev, and B. C. Sanders, Phys. Rev. A **85**, 050303(R) (2012).
[30] B. R. Lavoie, P. M. Leung, and B. C. Sanders, Phys. Rev. A **88**, 023860 (2013).
[31] C. Tan and G. Huang, Phys. Rev. A **89**, 033860 (2014).
[32] C. Tan and G. Huang, Phys. Rev. A **91**, 023803 (2015).
[33] Q. Liu, N. Li, and C. Tan, Phys. Rev. A **101**, 023818 (2020).
[34] S. Asgarnezhad-Zorgabad, R. Sadighi-Bonabi, and B. C. Sanders, Phys. Rev. A **98**, 013825 (2018).
[35] S. Asgarnezhad-Zorgabad, P. Berini, and B. C. Sanders, Phys. Rev. A **99**, 051802(R) (2019).
[36] D. V. Skryabin and A. V. Gorbach, Rev. Mod. Phys. **82**, 1287 (2010).
[37] M. Liu, A.-P. Luo, Z. C. Luo, and W. C. Xu, Opt. Lett. **42**, 330 (2017).
[38] Q. F. Yang, X. Yi, K. Y. Yang, and K. Vahala, Nat. Phys. **13**, 53 (2017).
[39] L. Karpa and M. Weitz, Nat. Phys. **2**, 332 (2006).
[40] Z. Chen and G. Huang, Phys. Rev. A **89**, 033817 (2014).
[41] Z. Chen, H. Xie, Q. Li, and G. Huang, Phys. Rev. A **100**, 013827 (2019).
[42] C. Tan and G. Huang, J. Opt. Soc. Am. B **31**, 704 (2014).
[43] S. J. Orfanidis, *Electromagnetic Waves and Antennas* (Rutgers University, New Brunswick, NJ, 2002).
[44] E. Figueroa, F. Vewinger, J. Appel, and A. I. Lvovsky, Opt. Lett. **31**, 2625 (2006).
[45] G. Huang, L. Deng, and M. G. Payne, Phys. Rev. E **72**, 016617 (2005).
[46] D. A. Steck, Rubidium 87 D Line Data, http://steck.us/alkalidata.
[47] Y. S. Kivshar and G. Agrawal, *Optical Solitons: From Fibers to Photonic Crystals* (Academic Press, 2003).
[48] E. H. Majid, K. M. F. Mohammad, and Z. Abbas, Appl. Opt. **48**, 5005 (2009).